

Dimerization-enhanced exotic magnetization plateau and magnetoelectric phase diagrams in skew-chain $\text{Co}_2\text{V}_2\text{O}_7$

Z. H. Li,^{1,2} X. T. Han,^{1,2} C. Dong,¹ H. W. Wang,¹ Z. Z. He,³ R. Chen,⁴ W. X. Liu,¹ C. L. Lu,¹ Y. Kohama^{①,5}, M. Tokunaga^{①,5}, K. Kindo,⁵ Z. W. Ouyang,¹ J. F. Wang,¹ and M. Yang^{①,1,*}


¹Wuhan National High Magnetic Field Center and School of Physics, Huazhong University of Science and Technology, Wuhan 430074, China

²State Key Laboratory of Advanced Electromagnetic Engineering and Technology, Huazhong University of Science and Technology, Wuhan 430074, China

³State Key Laboratory of Structural Chemistry, Fujian Institute of Research on the Structure of Matter, Chinese Academy of Sciences, Fuzhou, Fujian 350002, China

⁴College of Physics and Electronic Engineering, Xinyang Normal University, Xinyang 464000, China

⁵The Institute for Solid State Physics (ISSP), University of Tokyo, Chiba 277-8581, Japan

 (Received 15 August 2023; revised 12 January 2024; accepted 27 February 2024; published 22 March 2024)

The low-dimensional frustrated antiferromagnet system has been an appealing playground for investigating the exotic magnetic ground states. The $S = 1/2$ skew chain $\text{Co}_2\text{V}_2\text{O}_7$ attracted considerable interest for its magnetization plateau and the emergent ferroelectricity under high magnetic fields. In this work, we report the comprehensive angular studies of the magnetization plateau and the ferroelectric polarization in $\text{Co}_2\text{V}_2\text{O}_7$ under high fields up to 30 T. The magnetization was studied in detail with the applied field rotated within the bc and ab planes. We find that the $1/2$ magnetization plateau is enhanced with the field rotating within the bc plane and becomes most pronounced when the field is tilted 30° away from the b axis (denoted as the b^* axis). The temperature dependence of ferroelectric polarization was also studied along the a , c , and b^* axes, respectively. Based on these polarization measurements, the magnetic field temperature phase diagrams have been constructed for the three axes. We propose a model which considers the decoupling of the two inequivalent Co spins to explain the exotic polarization flop and the phase diagrams. This decoupling is considered to be enhanced by the dimerization effect, and that the non-negligible interchain interaction J_3 plays a crucial role.

DOI: [10.1103/PhysRevB.109.094432](https://doi.org/10.1103/PhysRevB.109.094432)

I. INTRODUCTION

Low dimensional frustrated magnets have been extensively regarded as a cornucopia to explore different quantum phases [1–3]. The spin frustration, originating from complex competition among various interactions, produces large degeneracy of the ground states and thus exotic properties such as the magnetization plateau, spin nematic, and longitudinal spin density wave states [4–9]. As one of the most celebrated quantum phases, magnetization plateaus have been observed in a variety of frustration systems with different geometries in low dimensional systems [10–14].

Among various magnetic structures, the one-dimensional spin chain has always been a classic example of frustrated magnet systems. Recently, the skew-chain system of the $R_2\text{V}_2\text{O}_7$ family ($R = \text{Ni}$ and Co) was reported to be a typical frustrated antiferromagnet system where a $1/2$ -magnetization plateau was observed under high fields [15–18]. For both compounds, they crystallize in a monoclinic structure (space group $P21/c$), with the skew chain formed by two series of nonequivalent edge-sharing octahedra of RO_6 along c and separated by nonmagnetic tetrahedrons VO_4 between the chains [Fig. 1(a)]. In the $S = 1$ $\text{Ni}_2\text{V}_2\text{O}_7$ chain system, unconven-

tional wide $1/2$ and $3/4$ magnetization plateaus have been observed under high magnetic field. The $1/2$ plateau was interpreted as the result of the weakly coupled $\text{Ni}2$ monomers, while the latter plateau is due to the dimerization of the $\text{Ni}1$ spins caused by the extremely strong interchain interaction [17].

For the case of $\text{Co}_2\text{V}_2\text{O}_7$, the antiferromagnetic interaction between Co spins, which are much weaker than that in $\text{Ni}_2\text{V}_2\text{O}_7$, gives rise to a frustrated $S = 1/2$ chain. It undergoes a transition to an antiferromagnetic (AFM) ordering at $T_N = 6.5$ K, where the Co spins are located in the bc plane in a noncollinear manner [19]. The moments of the two nonequivalent Co spins are revealed to be $2.06(5)\mu_B$ and $2.69(5)\mu_B$, respectively. The Co spins formed an “up-up-down-down” canting chain and the canting angle is around 26° off the b axis. Different from that in $\text{Ni}_2\text{V}_2\text{O}_7$, the interchain interaction J_3 is comparable to the intrachain interactions J_1 and J_2 . The $1/2$ magnetization was only observed along $H \parallel b$ as a consequence, while it is robust along all three crystalline axes in $\text{Ni}_2\text{V}_2\text{O}_7$ [15].

Another attractive aspect of $\text{Co}_2\text{V}_2\text{O}_7$ is the magnetoelectric (ME) phenomena which are attributed to the broken symmetric nature as in other type-II multiferroics which are of spin origin. Under magnetic fields, field-induced ferroelectric (FE) polarizations emerged along different directions when $H \parallel b$ for $T < T_N$ [19]. A few successive FE phases

*Corresponding author: ming_yang@hust.edu.cn

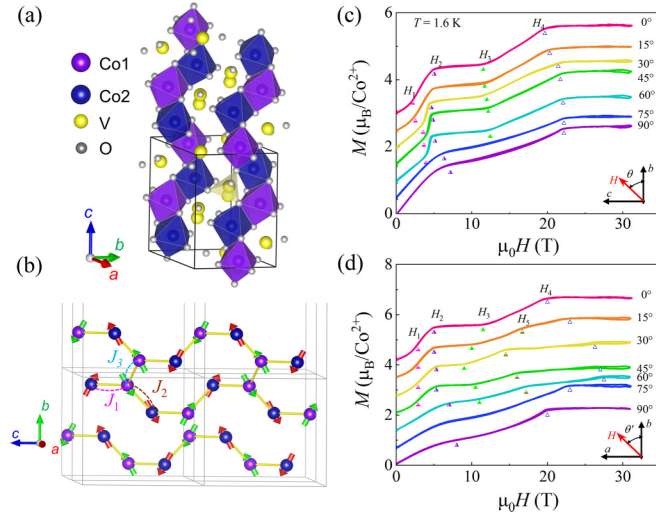


FIG. 1. (a) Crystal structure of $\text{Co}_2\text{V}_2\text{O}_7$ showing the skew chain structure along the c axis. Two different types of magnetic Co^{2+} ions are surrounded by six oxygen ions and form edge-sharing CoO_6 octahedra (purple and blue). (b) The schematic of the a axis projection of the Co networks in the skew-chain lattice of $\text{Co}_2\text{V}_2\text{O}_7$, showing the canted spin structure within the bc plane at low temperature ($T < T_N$) [19]. The intrachain interactions J_1 (3.0533 Å)/ J_2 (3.0335 Å) and interchain interaction J_3 (2.9727 Å) are indicated. (c),(d) The angular dependence of the magnetization as a function of magnetic field at 1.6 K. The magnetizations were measured as the magnetic field rotated from b to c axis (upper panel) and b to a axis (lower panel), respectively. All curves are vertically shifted for clarity.

have been revealed under magnetic field up to 25 T. In addition, significant polarization flop and reversal behaviors were both observed in this compound. In typical systems of perovskite RMnO_3 and RMn_2O_5 (R = rare earth ions) which host the polarization flop and reversal behaviors, the polarization was suspected to originate from the inversed Dzyaloshinskii-Moriya (DM) interaction (or the spin current mechanism) that P is proportional to the $e_{ij} \times (S_i \times S_j)$ [20,21]. Thus, the P flop or reversal is probably related to the flop or reversal of the vector spin chirality $C (= S_i \times S_j)$ [22,23]. In the case of $\text{Co}_2\text{V}_2\text{O}_7$, the mechanism of the field-induced ME behaviors was revealed to be the inversed DM effect, ensured by the perfect agreement with the magnetic properties. From this concern, the study of the ME properties under high fields provides another approach to unveil the spin structure in the regime where the neutron or nuclear magnetic resonance (NMR) measurements are impossible.

Even though previous studies only focused on the anisotropic magnetization along three principal axes, the angular dependent magnetizations deserve further investigations since the Co spins form a canted antiferromagnetic ordering in almost the bc plane [19]. Consequently, the application of magnetic fields with a tilting angle should give rise to quadratic evolution of the electric polarization, as well as the related polarization reversal behaviors. Here, we performed multiple experiments under pulsed magnetic fields up to 30 T, by combining the angular dependent magnetization, the magnetostriction, and electric polarization with field applied along different directions to explore the exotic magnetic spin

structure and related ME effects in the skew chain system under high field. From the systematic measurements, the ME phase diagrams along various field directions have been constructed. We propose a model considering the dimerization of the Co1 spins, which leads to a decoupling of the Co1 and Co2 spins, and thus they contribute to the different FE states. The low field FE I phase is induced by the cycloidal structure of monomer Co2 spins, while the FE II phase is a result of a conical structure of dimer Co1 spins. Moreover, the emergent linear ME effect and the low field switching effect, with field applied approach to its easy axis, opens incentives for future memory functionalities.

II. EXPERIMENT

The studied single crystals of $\text{Co}_2\text{V}_2\text{O}_7$ were grown by flux technique [24]. Based on the phase diagram of the $\text{CoO-V}_2\text{O}_5$ system, single crystals of $\text{Co}_2\text{V}_2\text{O}_7$ are grown using V_2O_5 as self-flux at a slow cooling rate. The quality of grown crystals was analyzed by x-ray powder diffraction (XRD). Cubic and platelike samples were cut along different crystalline axes for the magnetization and electric polarization measurements. High field magnetization measurements were performed by induction method under pulsed magnetic fields up to 30 T with the pulse duration time of 10 ms [25]. The field sweeping rate is approximately 6 kT/s. The absolute magnetization values were calibrated using a 7-T superconducting quantum interference device (SQUID) magnetometer (Quantum Design). The angular magnetization measurements were realized with the use of a series of quartz column with tilting cross sections see the Supplemental Material [26]). The polarizations P were probed by measuring and integrating the pyroelectric current during the pulses of field and under a bias electric field of 450 kV/m at low temperatures [27]. Prior to the polarization measurements, a poling process was performed with a poling electric field ($E = 450$ kV/m) applied during sample cooling for aligning the FE domains. Furthermore, the high field magnetostriction was measured by the optical method using fiber Bragg gratings (FBGs) [28].

III. EXPERIMENTAL RESULTS

A. Angular dependent magnetization

As a guide to search the exotic phase of $\text{Co}_2\text{V}_2\text{O}_7$, the angular magnetization properties have been firstly investigated. Figure 1(c) shows the magnetization properties of $\text{Co}_2\text{V}_2\text{O}_7$ at $T = 1.6$ K, with the magnetic field applied at various directions. Note that θ and θ' are described as the angle between the field direction and the b axis within the bc and ba plane, as illustrated in the insets, respectively. For $\theta = 0$, i.e., $H \parallel b$, the magnetization M vs H behavior is quite consistent with an earlier report [16]. It shows a series of distinct transitions at $H_1 \sim 2.8$ T, $H_2 \sim 5.1$ T, $H_3 \sim 13.9$ T, and $H_4 \sim 18.7$ T, which are well visualized as peaks in the dM/dH curves in the Supplemental Material [26]. A 1/2-magnetization plateau appears between $H_2 < H < H_3$ and the magnetization saturates at $H > H_4$. As the field is tilted towards the c axis, the magnetization behavior shows clear evolution as θ increases. An impressed finding is that M exhibits a steep increase before

the plateau is established with θ between 30° and 60° . The dM/dH curves for these angles reveal a very sharp peak, instead of the broad peak with shoulder for $\theta < 30^\circ$. This behavior is reminiscent of the steplike transition observed in some other frustrated magnets, which were attributed to a metamagnetic transition [5,11,29,30]. In the present case, it can be ascribed to the spin-flop transition at H_1 ($\parallel b$) for which it becomes most pronounced when the field is applied along $\theta = 30^\circ$. The appearance of the sharpened spin-flop transition between 30° and 60° is typical in uniaxial antiferromagnetic systems when the field is applied close to the easy axis within a limited angle range [31,32]. When θ is higher than 75° as the field approaches the c axis, the spin-flop transition and the $1/2$ -magnetization plateau become smoothed. Furthermore, the angular dependent dM/dH curves also show that the saturation fields H_4 are all shifting to higher field as the field is tilted away from the b axis.

On the other hand, when the magnetic field was rotated within the ba plane, the magnetic behaviors are totally different [Fig. 1(d)]. The steep increase, which appears before the plateau is established when $30^\circ < \theta < 60^\circ$, is no longer present. Instead, the transitions to the magnetization plateau are smoother for all the angles. Furthermore, the magnetization plateau becomes shorter as θ' increases and disappears for $\theta' > 60^\circ$. In addition, another plateaulike behavior around $3/4 M_S$ emerges at H_5 at $15^\circ < \theta' < 60^\circ$, which was responsible for a spin configuration “ $\uparrow\uparrow\uparrow\uparrow\uparrow\uparrow\downarrow$ ” when the field is applied parallel to the direction of the interchain interaction J_3 [16]. The appearance of the $3/4 M_S$ is reminiscent of that observed in the isostructural $\text{Ni}_2\text{V}_2\text{O}_7$, which was explained by the dimerization of Ni1 ions across adjacent chains due to the strong interchain interaction J_3 [17]. When θ' is higher than 75° , M increases monotonically to saturation with only one broad spin-flop transition appearing. The angular dependence of the saturation field is also much more complicated than that when the field is rotated within the ab plane. It first shifts to higher field as θ' increases to 30° and moves to lower field for $\theta' > 60^\circ$.

B. Magnetization, electric polarization, and magnetostriction along $H \parallel b^*$

In Figs. 2(a)–2(c), we plot the magnetization, polarizations, and magnetostriction vs H at 1.6 K with $H \parallel b^*$ axis, i.e., the magnetic field applied off the b axis by 30° within the bc plane, to show the interrelation between multiple properties. In Fig. 2(a), the magnetization and its derivatives reveal a series of transitions at H_1 – H_4 , which were noted by the dotted vertical lines. It is worth noting that both the increasing- and decreasing-sweep data are plotted simultaneously and they collapse on top of each other almost perfectly, showing negligibly weak hysteresis at the H_2 and H_3 transitions. We now turn to the magnetoelectric properties, that the electric polarization along three main principal axes P_a , P_b , and P_c were measured with $H \parallel b^*$. As shown in Fig. 2(b), as the magnetic field increases, P_a , P_b , and P_c all exhibit two FE phases, which we denote as FE I at $H < H_2$ and FE II at $H_3 < H < H_4$, respectively. The paraelectric phases coincide well with the magnetization plateau and saturation due to the lack of inversion symmetry breaking. Within the FE I phase,

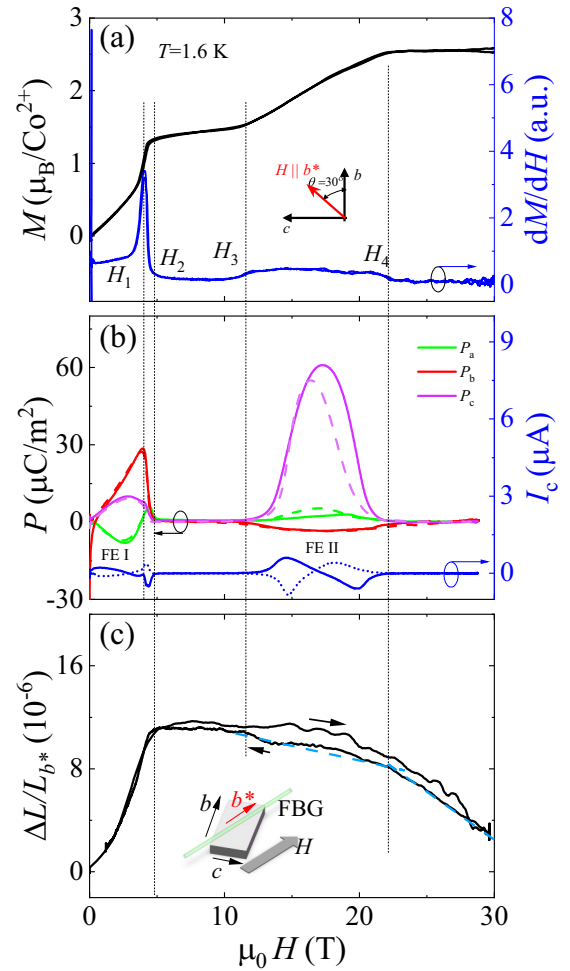


FIG. 2. (a) The high field magnetization along the b^* axis (the magnetic field was tilted 30° off the b axis in the bc plane) and its differential vs H at 1.6 K. (b) The polarization P_a , P_b , and P_c under $H \parallel b^*$ at 1.6 K. The pyroelectric current along c was also plotted, which corresponds to the P_c curve. The solid and dotted lines denote the data captured during decreasing and increasing sweeps, respectively. (c) The magnetostriction curves measured by the FBG method along the b^* axis at 1.6 K. The inset shows the measurement setup and the thick arrows indicate the field sweep direction.

P_a is negative until it changes its polarity at H_1 , while P_b and P_c are positive. Furthermore, the magnitudes of P_a and P_c are comparably small and half that of P_b . On the other hand, in the FE II phase, P_c reaches a maximum up to $60 \mu\text{C}/\text{m}^2$, whereas P_a and P_b are almost negligible, indicating a field-induced polarization flop to the c axis.

Additionally, the magnetostriction $\Delta L/L_{b^*}$ also shows the consistent transitions at the corresponding transitions. At low field for $H < H_2$, it increases up to 10 ppm in the same manner with the magnetization before the $1/2 M$ plateau is established. This behavior is consistent with the temperature dependence of the lattice parameter b determined by the neutron powder diffraction results, that it decreases upon cooling when the AFM ordering is formed [19]. As magnetic field is applied, the lattice parameter b should increase since the AFM ordering is suppressed. The elongation of b was confirmed by measuring

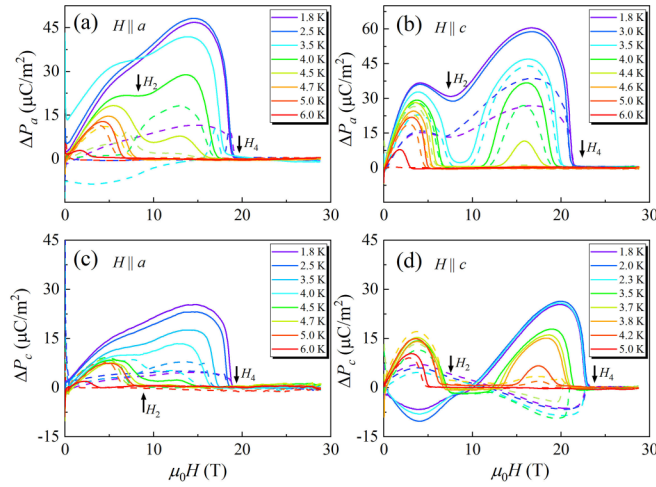


FIG. 3. The temperature-dependent electric polarization P_a and P_c for $H \parallel a$ and $H \parallel c$, respectively. The dashed lines denote the increasing sweeps of the field pulses and the solid lines the decreasing sweeps.

the magnetostriction along b with $H \parallel b$ for $H < H_2$ (shown in the Supplemental Material [26]), which is consistent with the magnetoelastic theory with the antiferromagnetic interactions being dominant [33]. At the magnetization plateau regime, it remains almost unchanged. At $H > H_3$, $\Delta L/L_{b^*}$ starts to decrease and changes its slope slightly at H_4 . Until the highest magnetic field, the magnetostriction does not show any sign of saturation and continues decreasing even when the magnetization saturates. The magnetostrictions along $H \parallel b$ also show similar nonmonotonic behavior with that of $H \parallel b^*$, except the value is one order of magnitude larger. This nonmonotonic evolution of magnetostriction and its contraction in the magnetization regime is unusual and cannot be explained by the normal magnetoelastic theory together with the distance of the various Co sites of different interactions. In this concern, we attribute it to the field-dependent contraction of the distance between adjacent chains. Further experimental and theoretical analysis of this behavior are desired.

C. Magnetoelectric properties along various magnetic field directions

The electric polarization properties are closely related to the spin structure under magnetic fields, based on the DM interaction. Under certain field directions, the isotropic magnetization process would produce exotic electric polarization behaviors under high fields [34–36]. Based on the indication of the angular dependent magnetization properties, we performed comprehensive measurements of P along different axes under various field directions for $H \parallel a$, $H \parallel c$, and $H \parallel b^*$.

Here, we first illustrate the profiles of P_a and P_c measured under $H \parallel a$ and $H \parallel c$ at various temperatures in Fig. 3, respectively. When $T = 1.6$ K, P_a increases gradually with H_a up to a maximum of $10 \mu\text{C}/\text{m}^2$ during the increasing sweep as shown in Fig. 3(a). Further increasing H , P_a shows a sudden drop and the system enters the paraelectric state at $H_4 \sim 18$ T, which is consistent with the saturation field of magnetization

that all the spins are aligned to the magnetic field and the inversion symmetry is preserved [Fig. 1(d)]. When the field sweeps back, the system enters the FE state with a much larger polarization compared to its counterpart during the increasing sweep, that the maximum value reaching $40 \mu\text{C}/\text{m}^2$. The large difference of the polarization magnitudes results in a pronounced hysteresis loop, which is probably due to the complex motion of the magnetic domain walls inside the sample. At $H_2 \sim 8$ T, a subtle inflection point appears and it shows good accordance with the magnetization inflection for $H \parallel a$ shown in Fig. 1(d). As the temperature increases, the transition at H_4 moves to lower field and vanishes at $T = 4.7$ K. Meanwhile, the transition at H_2 becomes more pronounced and separates the FE phase into two parts, named FE I and FE II. As T increases, FE II disappears $T = 4.7$ K, and FE I survives up to 5 K. On the other hand, the polarization along c for $H \parallel a$ at various temperatures is shown in Fig. 3(c). It is found that the profiles of P_c are almost the same as P_a , with the overall magnitude only one-third of P_a . For $T = 6$ K, both FE I and FE II disappear and the sample is always in the paraelectric phase.

On the other hand, the temperature dependent P_a and P_c measured under $H \parallel c$ are displayed in Figs. 3(b) and 3(d). As shown in Fig. 3(b), P_a under $H \parallel c$ is almost identical to that of $H \parallel a$ at low temperatures, with the inflection between the two FE phases more obvious. When $T = 3.5$ K, the FE I and FE II phases separate completely as the system enters a PE state between the two FE phases. FE II weakens upon increasing temperature and disappears at $T = 4.7$ K, which is consistent with that for $H \parallel a$. On the contrary, for $H \parallel c$ [shown in Fig. 3(d)], P_c is much different than its counterpart for $H \parallel a$. At $T = 1.8$ K, $P_c(H)$ shows a ∞ -like behavior, that the polarity of the FE II is opposite to FE I phase. Meanwhile, the polarities are also reversed between the increasing and decreasing sweeps. This polarization reversal phenomenon has also been found in the study of MnWO_4 [37] and TbMn_2O_5 [20]. As the temperature increases, the reversal between FE I and FE II disappears for $T > 2.2$ K, while the reversal between increasing and decreasing sweeps disappears at 3.7 K for FE II. Besides, at temperatures for $T \geq 3.5$ K, a plateau emerges between the positive and negative P and it extends to larger magnetic field range as T increases. This full separation of the two FE phases can be ascribed to the appearance of a $1/2$ magnetization plateau stabilized by thermal fluctuation at elevated temperatures [38].

Figure 4 illustrates the ME responses along the three axes under the $H \parallel b^*$ and at various temperatures, respectively. The polarization behaviors and their evolutions are distinctly different from that for $H \parallel a$ and $H \parallel c$. Most amazing is the obvious separation between the two FE phases that the FE II phase has its major component only along the c axis, whereas the FE I phase appears on the a and b axes. The lowest temperature $P(H)$ curves for the three directions all show corresponding transitions at the same fields and are in good agreement with the magnetization behavior, evidencing the magnetic origin of the ferroelectric polarization in CVO. In Fig. 4(a), P_a first shows a sawtoothlike behavior at low field for the lowest temperature with negative polarity. As the field increases, P_a enters the PE and FE II phase subsequently and the amplitude of the FE II phase is only a half of the

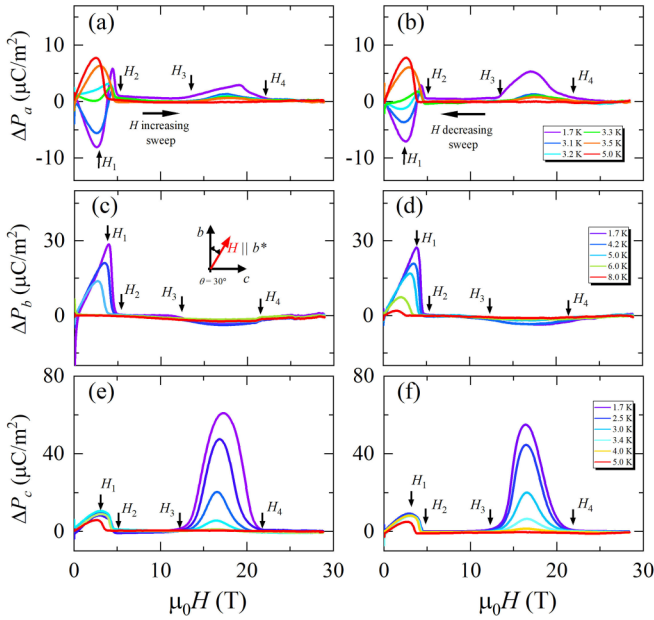


FIG. 4. (a)–(f) The temperature-dependent polarization along a , b , and c with the magnetic field applied along the b^* axis, respectively.

FE I phase. Upon warming, the negative P_a in the FE I state weakens and switches to positive with larger amplitudes. Notably, on the other hand, P_b exhibits a linear ME response as $H < H_1$, similar to that reported in other ME systems [39,40]. In the high field range, the polarization remains negligibly weak compared to its low field counterpart. On the contrary, P_c shows a much stronger polarization in the FE II state, while its FE I phase is comparable to P_a ($\sim 10 \mu\text{C}/\text{m}^2$) and half to P_b .

IV. DISCUSSION

Based on the angular dependent electric polarization data, we summarize the ME phase diagram for H applied along various directions for $\text{Co}_2\text{V}_2\text{O}_7$ in Fig. 5. Since the strong hysteresis and nonequilibrium effects during the field sweeps, we use only the polarization data captured during the decreasing field to extract the phase boundaries. With two basic FE phases existing, the present phase diagrams provide additional information compared to the previous one reported by Chen *et al.* [18]. As is well documented in Ref. [18], the polarizations manifest three FE phases when H is applied along the b axis. The FE-I and FE-II phases at lower fields are along the b axis, while the FE-III is along the ac plane due to a polarization flop effect from the FE-II phase.

As is clearly visualized in Fig. 5, the phase boundaries from the electric polarization match well with the magnetization transitions. The good agreements between the temperature dependencies of the electric polarization and the magnetization ensure that the ferroelectric polarization in $\text{Co}_2\text{V}_2\text{O}_7$ arises from the spin arrangement under magnetic field with different directions. Combined with the canted ground magnetic structure obtained from the neutron diffraction patterns

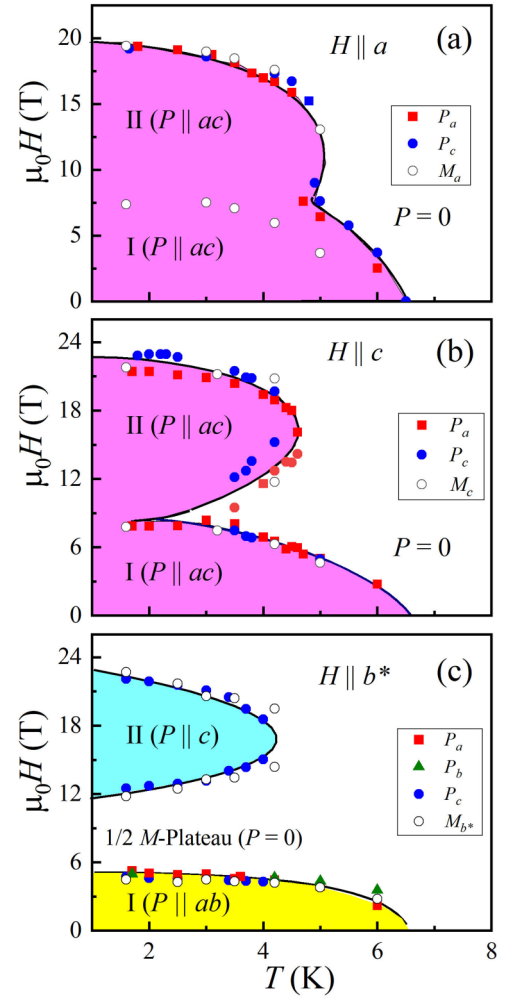


FIG. 5. The magneto-electric H - T phase diagram of $\text{Co}_2\text{V}_2\text{O}_7$ along the a , b , and b^* axes, respectively. The phase boundaries were extracted from the temperature-dependent polarization and magnetization transitions during the decreasing sweeps.

[19], we will now explain the exotic angular dependence of the magnetization and electric polarization behaviors in the present work.

We propose a model based on a decoupling effect between the Co1 and Co2 spins within one chain due to the presence of J_3 as shown in Fig. 6, which links the two Co1 ions between two adjacent chains. In the isostructural $\text{Ni}_2\text{V}_2\text{O}_7$, J_3 is much stronger than J_1 and J_2 ; as a result a pronounced dimerization between the Ni1 ions in two chains is responsible for the appearance of the $3/4$ -magnetization plateau under ultrahigh magnetic field. Back to the case of $\text{Co}_2\text{V}_2\text{O}_7$, as even J_3 is much weaker than that in $\text{Ni}_2\text{V}_2\text{O}_7$, it is possible to consider the dimerization effect as well. We propose that within $1/2$ magnetization plateau under $H \parallel b^*$ and b , the Co2 spins are first polarized along the external magnetic field, while the Co1 spins remain antiferromagnetically ordered due to a dimerization effect between chains. This hypothesis can be evidenced by the fact that the magnetic moment at the onset of $1/2$ plateau is $0.52 M_S$, which is can be attributed to the unequal moments of the Co1 ($2.06 \mu_B$) and Co2 ($2.69 \mu_B$) moments.

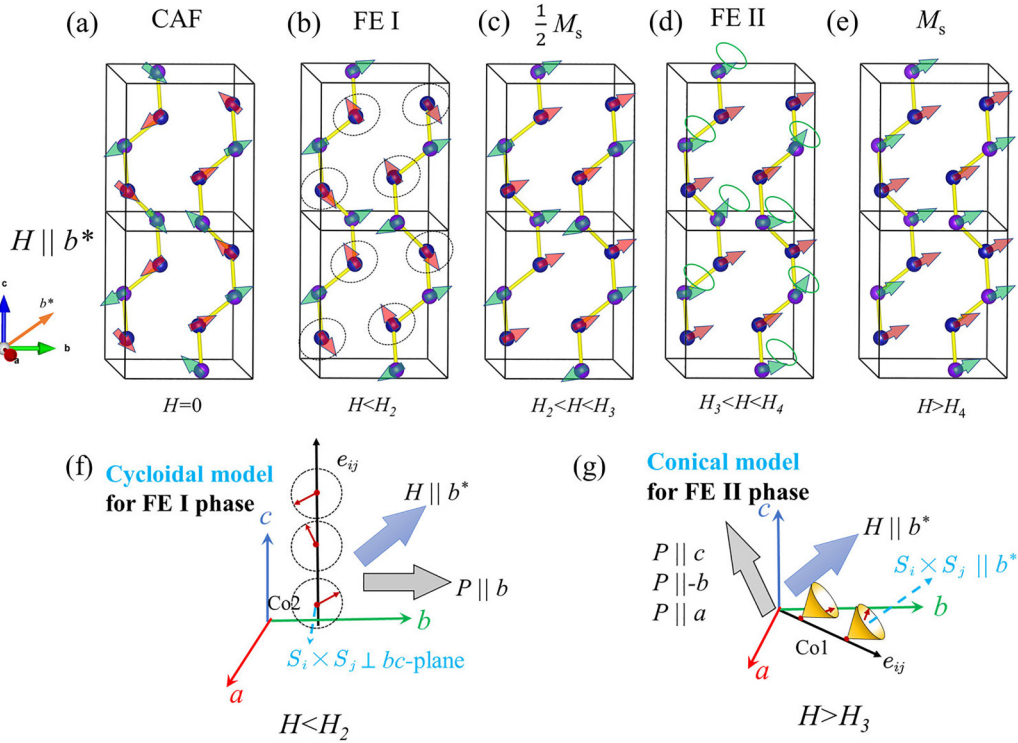


FIG. 6. Visualization of the magnetic structure of $\text{Co}_2\text{V}_2\text{O}_7$ for different ranges of $H \parallel b^*$: (a) the canted AFM state under $H = 0$; (b) the cycloidal structure of Co2 spins corresponds to the FE I phase; (c) the $1/2$ plateau state (PE state); (d) the conical structure of Co1 spins related to the FE II phase; (e) the magnetic saturation state with all the spins fully polarized (PE phase). Panels (f) and (g) illustrate the detailed inversed DM model of the cycloidal structure of Co2 and the conical structure of Co1, which are responsible for the FE I and FE II phases, respectively. The red arrows indicate the Co2 spins and the green ones are Co1 spins.

Thus, the magnetization process before the $1/2$ plateau ($H < H_2$) is mainly related to the spin alignment of the Co2 spins and the one between the $1/2$ plateau and saturation is the polarization of Co1 spins. Using this model one can achieve a qualitative description of the ME phases for $H \parallel b^*$.

As shown in Fig. 6(b), the Co2 spins form a cycloidal structure within the bc plane due to the moderate anisotropy in $\text{Co}_2\text{V}_2\text{O}_7$ [41]. Therefore, a FE with the most components along the b axis is reduced through the inversed DM effect, that the $S_i \times S_j$ is perpendicular to the bc plane and $e_{ij} \parallel c$ axis [Fig. 6(f)]. The maximum magnitudes of the polarizations are reached at H_2 where a spin flop occurs, that the cycloidal structure is suppressed. On the other hand, for $H_2 < H < H_4$, the Co1 spins form an equivalent spin chain along the direction of J_3 , that the spin-connected wave vector $e_{ij} = (0.3, 0.25, -0.07)$ [Fig. 6(g)]. Along the new chain, which is approximately lying within the ab plane, a conical structure is formed with its chiral vector along the b^* axis. Then the main component of the polarization is along the c axis. This spin structure concerning the flop of the spin-connecting vector is also applicable to the cases of $H \parallel b$ axis, that the P_b in the low field FE I phase flops into the ac plane. On the other hand, for $H \parallel a$ and $H \parallel c$ axes, the fact that FE I and FE II are connected to each other at low temperature but separate at elevated temperatures, as well as their different temperature dependence of the polarization magnitudes, would also be a possible indication that they are from different sublattices of the Co spins. Proposed by Chen *et al.* very recently [38],

this separation of FE I and FE II phases was attributed to the existence of a possible quantum critical region, that the dimerization of Co1-Co1 is stabilized due to the enhanced contribution of J_3 at higher temperatures when $H \parallel c$ axis.

V. SUMMARY

Overall, we have explored the angular-dependent magnetization and magnetoelectric effect of a $S = 1/2$ skew chain $\text{Co}_2\text{V}_2\text{O}_7$, complemented by magnetostriction measurements up to 30 T. Our results provide strong support for the correlation between the spin orders and the magnetoelectric effects in this skew chain system under magnetic fields. The $1/2$ magnetization plateau appearing at $H \parallel b$ becomes more pronounced when H is rotated to the b^* , which is related to the tilting angle of the canted AFM ground state. The electric polarization along different axes under various magnetic fields is also systematically studied, from which we construct the ME phase diagrams for $H \parallel a$, c , and b^* axes. Specifically, we reveal a full separation of the FE phases due to the polarization flop. Within the frame of inversed DM mechanism, we proposed a model based on the decoupling of the Co1 and Co2 spins to explain the origins of the exotic magnetoelectric properties. The non-negligible interchain interaction J_3 plays a crucial role in determining the complex magnetoelectric phase diagram of the skew chain system $\text{Co}_2\text{V}_2\text{O}_7$.

ACKNOWLEDGMENTS

This work was supported by the National Natural Science Foundation of China (Grants No. 12074135, No. 12104351, No. 11774106, No. 12004122, No. 12104388, and No.

21875249), the Hubei Province Natural Science Foundation of China (Grant No. 2021CFB027 and No. 2020CFA083), and the China Postdoctoral Science Foundation (Grant No. 2023M731209).

- [1] P. A. Lee, An end to the drought of quantum spin liquids, *Science* **321**, 1306 (2008).
- [2] L. Balents, Spin liquids in frustrated magnets, *Nature (London)* **464**, 199 (2010).
- [3] O. A. Starykh, Unusual ordered phases of highly frustrated magnets: A review, *Rep. Prog. Phys.* **78**, 052502 (2015).
- [4] Y. Shirata, H. Tanaka, A. Matsuo, and K. Kindo, Experimental realization of a spin-1/2 triangular-lattice Heisenberg antiferromagnet, *Phys. Rev. Lett.* **108**, 057205 (2012).
- [5] S. Imajo, N. Matsuyama, T. Nomura, T. Kihara, S. Nakamura, C. Marcenat, T. Klein, G. Seyfarth, C. Zhong, H. Kageyama *et al.*, Magnetically hidden state on the ground floor of the magnetic devil's staircase, *Phys. Rev. Lett.* **129**, 147201 (2022).
- [6] A. Orlova, E. L. Green, J. M. Law, D. I. Gorbunov, G. Chanda, S. Krämer, M. Horvatić, R. K. Kremer, J. Wosnitzer, and G. L. J. A. Rikken, Nuclear magnetic resonance signature of the spin-nematic phase in LiCuVO_4 at high magnetic fields, *Phys. Rev. Lett.* **118**, 247201 (2017).
- [7] Y. Kohama, H. Ishikawa, A. Matsuo, K. Kindo, N. Shannon, and Z. Hiroi, Possible observation of quantum spin-nematic phase in a frustrated magnet, *Proc. Natl. Acad. Sci. USA* **116**, 10686 (2019).
- [8] O. A. Starykh and L. Balents, Excitations and quasi-one-dimensionality in field-induced nematic and spin density wave states, *Phys. Rev. B* **89**, 104407 (2014).
- [9] S. Kimura, M. Matsuda, T. Masuda, S. Hondo, K. Kaneko, N. Metoki, M. Hagiwara, T. Takeuchi, K. Okunishi, Z. He *et al.*, Longitudinal spin density wave order in a quasi-1D ising-like quantum antiferromagnet, *Phys. Rev. Lett.* **101**, 207201 (2008).
- [10] T. Ono, H. Tanaka, H. Aruga Katori, F. Ishikawa, H. Mitamura, and T. Goto, Magnetization plateau in the frustrated quantum spin system Cs_2CuBr_4 , *Phys. Rev. B* **67**, 104431 (2003).
- [11] H. Ishikawa, M. Yoshida, K. Nawa, M. Jeong, S. Krämer, M. Horvatić, C. Berthier, M. Takigawa, M. Akaki, A. Miyake *et al.*, One-third magnetization plateau with a preceding novel phase in volborthite, *Phys. Rev. Lett.* **114**, 227202 (2015).
- [12] S. Yoshii, T. Yamamoto, M. Hagiwara, S. Michimura, A. Shigekawa, F. Iga, T. Takabatake, and K. Kindo, Multistep magnetization plateaus in the shastry-sutherland system TbB_4 , *Phys. Rev. Lett.* **101**, 087202 (2008).
- [13] J. Wang, M. Tokunaga, Z. Z. He, J. I. Yamaura, A. Matsuo, and K. Kindo, High magnetic field induced phases and half-magnetization plateau in the $S = 1$ kagome compound $\text{Ni}_3\text{V}_2\text{O}_8$, *Phys. Rev. B* **84**, 220407(R) (2011).
- [14] K. Penc, N. Shannon, and H. Shiba, Half-magnetization plateau stabilized by structural distortion in the antiferromagnetic Heisenberg model on a pyrochlore lattice, *Phys. Rev. Lett.* **93**, 197203 (2004).
- [15] Z. W. Ouyang, Y. C. Sun, J. F. Wang, X. Y. Yue, R. Chen, Z. X. Wang, Z. Z. He, Z. C. Xia, Y. Liu, and G. H. Rao, Novel half-magnetization plateau and nematiclike transition in the $S = 1$ skew chain $\text{Ni}_2\text{V}_2\text{O}_7$, *Phys. Rev. B* **97**, 144406 (2018).
- [16] L. Yin, Z. W. Ouyang, J. F. Wang, X. Y. Yue, R. Chen, Z. Z. He, Z. X. Wang, Z. C. Xia, and Y. Liu, Anisotropic magnetization plateaus in $S_{\text{eff}} = 1/2$ skew-chain single-crystal $\text{Co}_2\text{V}_2\text{O}_7$, *Phys. Rev. B* **99**, 134434 (2019).
- [17] J. J. Cao, Z. W. Ouyang, X. C. Liu, T. T. Xiao, Y. R. Song, J. F. Wang, Y. Ishii, X. G. Zhou, and Y. H. Matsuda, Unusual dimerization and magnetization plateaus in $S = 1$ skew chain $\text{Ni}_2\text{V}_2\text{O}_7$ observed at 120 T, *Phys. Rev. B* **106**, 184409 (2022).
- [18] R. Chen, J. F. Wang, Z. W. Ouyang, M. Tokunaga, A. Y. Luo, L. Lin, J. M. Liu, Y. Xiao, A. Miyake, Y. Kohama *et al.*, Successive electric-polarization switches in the $S = 1/2$ skew chain $\text{Co}_2\text{V}_2\text{O}_7$ induced by a high magnetic field, *Phys. Rev. B* **100**, 140403(R) (2019).
- [19] W. H. Ji, L. Yin, W. M. Zhu, C. M. N. Kumar, C. Li, H.-F. Li, W. T. Jin, S. Nandi, X. Sun, Y. Su *et al.*, Noncollinear magnetic structure and anisotropic magnetoelastic coupling in cobalt pyrovanadate $\text{Co}_2\text{V}_2\text{O}_8$, *Phys. Rev. B* **100**, 134420 (2019).
- [20] N. Hur, S. Park, P. A. Sharma, J. S. Ahn, S. Guha, and S.-W. Cheong, Electric polarization reversal and memory in a multiferroic material induced by magnetic fields, *Nature (London)* **429**, 392 (2004).
- [21] T. Kimura, T. Goto, H. Shintani, K. Ishizaka, T. Arima, and Y. Tokura, Magnetic control of ferroelectric polarization, *Nature (London)* **426**, 55 (2003).
- [22] M. Fukunaga, Y. Sakamoto, H. Kimura, Y. Noda, N. Abe, K. Taniguchi, T. Arima, S. Wakimoto, M. Takeda, K. Kakurai *et al.*, Magnetic-field-induced polarization flop in multiferroic TmMn_2O_5 , *Phys. Rev. Lett.* **103**, 077204 (2009).
- [23] F. Kagawa, M. Mochizuki, Y. Onose, H. Murakawa, Y. Kaneko, N. Furukawa, and Y. Tokura, Dynamics of multiferroic domain wall in spin-cycloidal ferroelectric DyMnO_3 , *Phys. Rev. Lett.* **102**, 057604 (2009).
- [24] Z. He, J.-I. Yamaura, Y. Ueda, and W. Cheng, Magnetic properties of $\text{Co}_2\text{V}_2\text{O}_7$ single crystals grown by flux method, *J. Solid State Chem.* **182**, 2526 (2009).
- [25] J. Xie, S. Zhang, J. Shi, J. Wang, L. Li, and X. Han, Realisation of the reconfigurable pulsed high magnetic field facility and its scientific application at Wuhan National Pulsed High Magnetic Field Centre, *High Voltage* **8**, 898 (2023).
- [26] See Supplemental Material at <http://link.aps.org/supplemental/10.1103/PhysRevB.109.094432> for the quartz columns used in the angular magnetization measurements, the angular and temperature dependent magnetizations, the magnetostrictions, and the spin structure model for the FE II state.
- [27] R. Chen, J. F. Wang, Z. W. Ouyang, Z. Z. He, S. M. Wang, L. Lin, J. M. Liu, C. L. Lu, Y. Liu, C. Dong *et al.*, Magnetic field induced ferroelectricity and half magnetization plateau in polycrystalline $\text{R}_2\text{V}_2\text{O}_8$ ($\text{R}=\text{Ni}, \text{Co}$), *Phys. Rev. B* **98**, 184404 (2018).

- [28] R. Daou, F. Weickert, M. Nicklas, F. Steglich, A. Haase, and M. Doerr, High resolution magnetostriction measurements in pulsed magnetic fields using fiber bragg gratings, *Rev. Sci. Instrum.* **81**, 033909 (2010).
- [29] H. Ueda, H. A. Katori, H. Mitamura, T. Goto, and H. Takagi, Magnetic-field induced transition to the 1/2 magnetization plateau state in the geometrically frustrated magnet CdCr_2O_4 , *Phys. Rev. Lett.* **94**, 047202 (2005).
- [30] V. Felea, P. T. Cong, L. Prodan, D. I. Gorbunov, T. Nomura, Y. Skourski, S. Zherlitsyn, J. Wosnitza, Zhaosheng Wang, A. Miyata *et al.*, High-field phase transitions in the orbitally ordered multiferroic GeV_4S_8 , *Phys. Rev. B* **101**, 064413 (2020).
- [31] Z. W. Ouyang, V. K. Pecharsky, K. A. Gschneidner, D. L. Schlagel, and T. A. Lograsso, Angular dependence of the spin-flop transition and a possible structure of the spin-flop phase of Gd_5Ge_4 , *Phys. Rev. B* **76**, 134415 (2007).
- [32] K. W. Blazey, H. Rohrer, and R. Webster, Magnetocaloric effects and the angular variation of the magnetic phase diagram of antiferromagnetic GdAlO_3 , *Phys. Rev. B* **4**, 2287 (1971).
- [33] V. S. Zapf, V. F. Correa, P. Sengupta, C. D. Batista, M. Tsukamoto, N. Kawashima, P. Egan, C. Pantea, A. Migliori, and J. B. Bettset al., Direct measurement of spin correlations using magnetostriction, *Phys. Rev. B* **77**, 020404(R) (2008).
- [34] L. Ponet, S. Artyukhin, Th. Kain, J. Wettstein, A. Pimenov, A. Shuvaev, X. Wang, S.-W. Cheong, M. Mostovoy, and A. Pimenov, Topologically protected magnetoelectric switching in a multiferroic, *Nature (London)* **607**, 81 (2022).
- [35] C. Dong, J. F. Wang, Z. Z. He, Y. T. Chang, M. Y. Shi, Y. R. Song, S. M. Jin, Y. Q. Du, Z. Y. Wu *et al.*, Reentrant ferroelectric phase induced by a tilting high magnetic field in $\text{Ni}_3\text{V}_2\text{O}_8$, *Phys. Rev. B* **105**, 024427 (2022).
- [36] J. F. Wang, W. X. Liu, Z. Z. He, C. B. Liu, M. Tokunaga, M. Li, C. Dong, X. T. Han, F. Herlach, C. L. Lu *et al.*, Ferroelectric polarization reversal in multiferroic mnwo_4 via a rotating magnetic field up to 52 T, *Phys. Rev. B* **104**, 014415 (2021).
- [37] H. Mitamura, T. Sakakibara, H. Nakamura, T. Kimura, and K. Kindo, Multiferroicity on the zigzag-chain antiferromagnet MnWO_4 in high magnetic fields, *J. Phys. Soc. Jpn.* **81**, 054705 (2012).
- [38] R. Chen, H. J. Hu, Q. K. Lei, C. B. Liu, C. Dong, X. Y. Yue, Z. Qu, H. W. Wang, Y. Qiu, D. Chen *et al.*, Ferroelectricity and multiferroic quantum critical behaviors in $\text{Co}_2\text{V}_2\text{O}_7$, *Phys. Rev. B* **108**, 224405 (2023).
- [39] Y. Chang, J. Wang, W. Wang, C. Liu, B. You, M. Liu, S. Zheng, M. Shi, C. Lu, and J.-M. Liu, Linear magnetoelectric memory and training effect in the honeycomb antiferromagnet $\text{Co}_4\text{Nb}_2\text{O}_9$, *Phys. Rev. B* **107**, 014412 (2023).
- [40] V. Kocsis, Y. Tokunaga, Y. Tokura, and Y. Taguchi, Switching of antiferromagnetic states in LiCoPO_4 as investigated via the magnetoelectric effect, *Phys. Rev. B* **104**, 054426 (2021).
- [41] O. I. Utesov and A. V. Syromyatnikov, Formation of spiral ordering by magnetic field in frustrated anisotropic antiferromagnets, *Phys. Rev. B* **100**, 054439 (2019).